AGU PUBLICATIONS

Geochemistry, Geophysics, Geosystems

RESEARCH ARTICLE
10.1002/2016GC006660

Iron isotopic evolution during fractional crystallization of the uppermost Bushveld Complex layered mafic intrusion

Laura D. Bilenker[1,2], Jill A. VanTongeren[3], Craig C. Lundstrom[4], and Adam C. Simon[1]

[1]Department of Earth and Environmental Sciences, University of Michigan, Ann Arbor, Michigan, USA, [2]Now at Department of Earth, Ocean, and Atmospheric Sciences, Pacific Centre for Isotopic and Geochemical Research, University of British Columbia, Vancouver, BC, V6T 1Z4, Canada, [3]Department of Earth and Planetary Sciences, Rutgers University, Wright Geological Laboratory 343, Piscataway, New Jersey, USA, [4]Department of Geology, University of Illinois, Champaign, Illinois, USA

Key Points:
- Whole rock and magnetite separates from the uppermost portion of the Bushveld Complex were analyzed for their Fe isotope compositions
- We find no systematic variation in whole rock or magnetite Fe isotope ratios with stratigraphic height
- 85% crystallization of a dry tholeiitic multiply-saturated magma does not significantly fractionate Fe isotopes

Supporting Information:
- Supporting Information S1
- Table S1

Correspondence to:
L. Bilenker,
bilenker@umich.edu

Citation:
Bilenker, L. D., J. A. VanTongeren, C. C. Lundstrom, and A. C. Simon (2017), Iron isotopic evolution during fractional crystallization of the uppermost Bushveld Complex layered mafic intrusion, *Geochem. Geophys. Geosyst.*, *18*, doi:10.1002/2016GC006660.

Received 28 SEP 2016
Accepted 9 FEB 2017
Accepted article online 16 FEB 2017

Abstract We present δ^{56}Fe (^{56}Fe/^{54}Fe relative to standard IRMM-014) data from whole rock and magnetite of the Upper and Upper Main Zones (UUMZ) of the Bushveld Complex. With it, we assess the role of fractional crystallization in controlling the Fe isotopic evolution of a mafic magma. The UUMZ evolved by fractional crystallization of a dry tholeiitic magma to produce gabbros and diorites with cumulus magnetite and fayalitic olivine. Despite previous experimental work indicating a potential for magnetite crystallization to drastically change magma δ^{56}Fe, we observe no change in whole rock δ^{56}Fe above and below magnetite saturation. We also observe no systematic change in whole rock δ^{56}Fe with increasing stratigraphic height, and only a small variation in δ^{56}Fe in magnetite separates above magnetite saturation. Whole rock δ^{56}Fe (errors twice standard deviation, $\pm 2\sigma$) throughout the UUMZ ranges from $-0.01 \pm 0.03‰$ to $0.21 \pm 0.09‰$ ($\delta^{56}Fe_{averageWR} = 0.10 \pm 0.09‰$; n = 21, isotopically light outlier: $\delta^{56}Fe_{WR} = -0.15‰$), and magnetites range from $0.28 \pm 0.04‰$ to $0.86 \pm 0.07‰$ ($\delta^{56}Fe_{averageMgt} = 0.50 \pm 0.15‰$; n = 20), similar to values previously reported for other layered intrusions. We compare our measured $\delta^{56}Fe_{WR}$ to a model that incorporates the changing normative mineralogy, calculated temperatures, and published fractionation factors of Fe-bearing phases throughout the UUMZ and produces $\delta^{56}Fe_{WR}$ values that evolve only in response to fractional crystallization. Our results show that the Fe isotopic composition of a multiply saturated (multiple phases on the liquidus) magma is unlikely to change significantly during fractional crystallization of magnetite due to the competing fractionation of other Fe-bearing cumulus phases.

1. Introduction

Significant variations of stable Fe isotope ratios are predicted to occur under magmatic/magmatic-hydrothermal conditions (i.e., high T, P) [e.g., *Shahar et al*., 2008]. Proposed magmatic processes leading to isotopic fractionation include fractional crystallization [e.g., *Schuessler et al*., 2007, 2009; *Teng et al*., 2008], fluid exsolution [*Poitrasson and Freydier*, 2005; *Heimann et al*., 2008; *Telus et al*., 2012], changes in oxygen fugacity (fO_2) [*Williams et al*., 2005; *Sossi et al*., 2012, *Foden et al*., 2015], bonding environment [e.g., *Dauphas et al*., 2014; *Sossi and O'Neill*, 2017], and thermal gradients [*Lundstrom*, 2009; *Huang et al*., 2010; *Zambardi et al*., 2014].

Several of these processes are likely at play in a magmatic/magmatic-hydrothermal system during and after its formation, and the Fe isotope signature of whole rock samples will reflect all of them. Iron isotope fractionation factors among mineral, melt, and aqueous fluid have been determined by analyses of natural and experimental samples, as well as estimated theoretically. Using these published fractionation factors, it is possible to combine these data with field, petrological, and additional geochemical observations to elucidate the contributions of individual processes to the measured Fe isotope ratio of a sample. Isolating processes by studying a controlled experimental or closed natural system can help advance our understanding of Fe isotope fractionation at magmatic/magmatic-hydrothermal conditions and in turn improve our ability to interpret the geologic history of a deposit or intrusion based upon the Fe isotope composition of rocks and minerals.

Schuessler et al. [2007], *Shahar et al*. [2008], and *Sossi and O'Neill* [2017] are the only published experimental studies to date conducted at conditions relevant to igneous systems. This is significant because such high-temperature experimental studies allow for direct measurement of isotope fractionation factors at conditions approaching equilibrium between crystals and liquid. The studies of *Schuessler et al*. [2007] and *Shahar et al*. [2008] demonstrated that Fe isotopes should fractionate in igneous systems due to the crystallization of individual mineral phases as well as due to magmatic redox processes. In the first published high-temperature experimental Fe isotope fractionation study, *Schuessler et al*. [2007] found that pyrrhotite ($Fe_{1-x}S$) preferentially incorporates isotopically light Fe by an average fractionation factor ($\Delta^{56}Fe_{pyrrhotite\text{-}melt}$) of about 0.35‰ relative to a silicic melt with ~62% Fe^{3+} between 800°C and 1000°C. Similarly, *Shahar et al*. [2008] performed experiments that demonstrated that magnetite is isotopically heavy relative to fayalite and quantified the amount of equilibrium fractionation between the two phases over a range of magmatic/magmatic-hydrothermal temperatures. The results of these studies are consistent with expectations based on the fact that the Fe in the pyrrhotite and fayalite structures is Fe^{2+} while the Fe in magnetite is mostly Fe^{3+}, although other factors such as ligand strength (e.g., Fe is bonded to S in pyrrhotite) also play a role.

Theoretical studies predicted this correlation between higher valence and heavier isotopic composition [e.g., *Polyakov and Mineev*, 2000; *Polyakov et al*., 2007], and the force constant measurements and subsequent modeling of *Dauphas et al*. [2014] is also consistent with Fe isotope fractionation being connected to redox and bonding environment. In the most recent experimental study on stable Fe isotope fractionation in magmatic systems, *Sossi and O'Neill* [2017] performed piston-cylinder experiments between a $FeCl_2$-bearing fluid and various minerals within which Fe^{2+} exists in VIII, VI, IV coordination. Magnetite, which contains Fe^{3+} in addition to Fe^{2+} and therefore has Fe in a mix of VI and IV coordination, was the isotopically heaviest mineral in the study. Their work provides further evidence that coordination number and bond length control fractionation.

The above experimental data are also consistent with field-based observations, such as those of *Sossi et al*. [2012]. Iron isotope data from the Red Hill sill supports a hypothesis that couples redox and fractional crystallization. *Sossi et al*. [2012] sampled stratigraphically throughout the 420 m thick sill in Tasmania, which is thought to have formed by a single intrusive event. The system was assumed closed to O_2 and experienced fractional crystallization. The whole rock data for the Red Hill sill show a trend toward isotopically heavy compositions early during the crystallization of pyroxene, which peak at magnetite saturation, and then become systematically lighter during magnetite crystallization (i.e., isotopically light Fe is removed from the melt by pyroxene and isotopically heavy Fe is removed from the melt by magnetite).

Teng et al. [2008] was the first study to present evidence in natural rocks for Fe isotope fractionation during fractional crystallization. By analyzing whole rocks and mineral separates from Kilauea Iki, Hawaii, USA, they showed that olivine, which preferentially incorporates Fe^{2+}, is isotopically lighter than a coexisting melt with respect to Fe isotopes. Later work on Kilauea Iki olivine phenocrysts combined Mg isotope measurements and Mg/Fe ratios with Fe isotope data [*Teng et al*., 2011]. The resulting modeling suggested that the olivine grains might be isotopically light with respect to Fe due to the ability of lighter isotopes to diffuse faster than heavier isotopes during magmatic differentiation. *Schuessler et al*. [2009] also focused on natural samples during their study on the dacitic and rhyolitic eruption products of Hekla volcano in Iceland. The Fe isotope compositions of the rhyolite samples were isotopically heavy compared to the dacite samples. Due to a lack of evidence for extensive fluid exsolution, the authors concluded that the difference in isotopic composition between the two groups of samples reflected fractional crystallization as the magma evolved from a dacite to a rhyolite; however no fractionating phase assemblage was specified to make this a quantitative model. Indeed, the original premise of *Poitrasson and Freydier* [2005] that there exists a strong hyperbolic increase toward heavier Fe isotopes in higher silica igneous rocks is clearly supported by the global database [e.g., *Heimann et al*., 2008; *Schuessler et al*., 2009; *Teng et al*., 2011; *Sossi et al*., 2012; *Foden et al*., 2015].

1.1. Iron Isotopes in Layered Mafic Intrusions

Despite these important studies, the mechanisms that control Fe isotope fractionation are still being actively investigated [e.g., *Young et al*., 2015], and little work has been done to apply Fe isotopes as a tool for studying the processes that form layered mafic intrusions [*Schoenberg et al*., 2009; *Chen et al*., 2014; *Liu et al*. 2014].

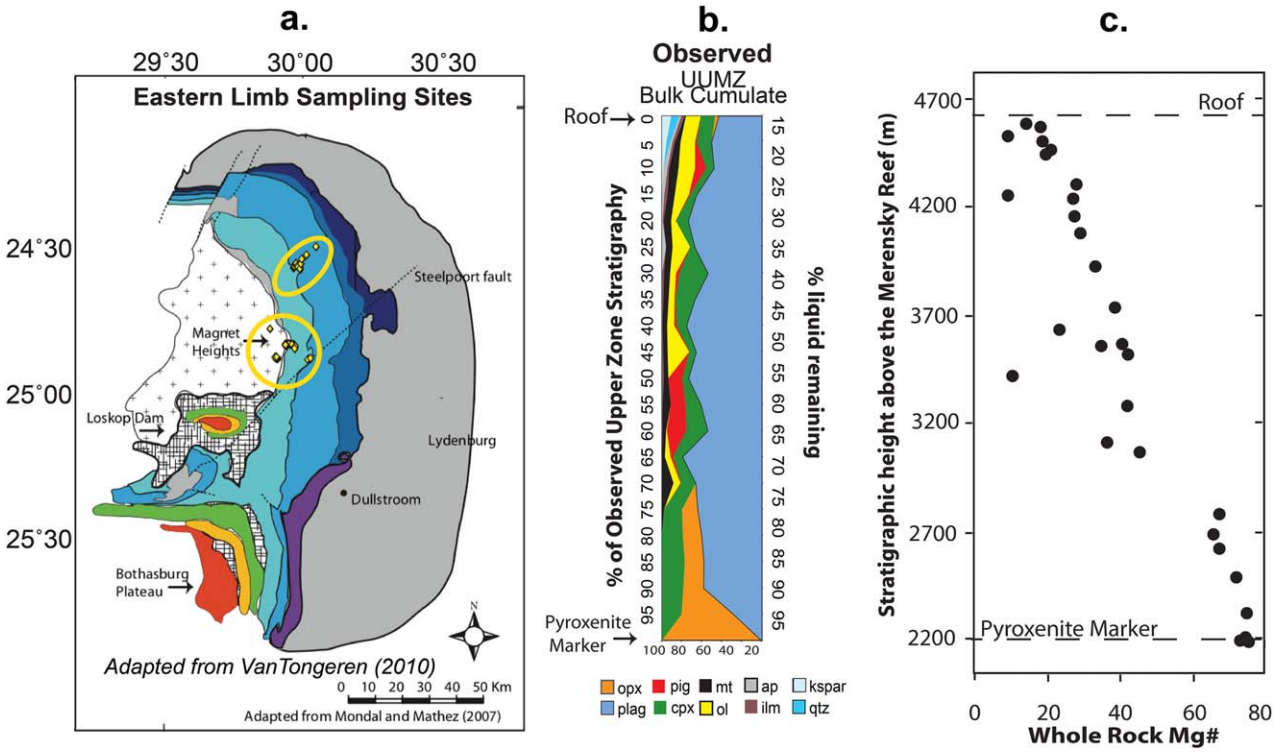

Figure 1. (a) geologic map of the Bushveld Complex and sampling sites for this study; (b) observed modal mineralogy throughout the UUMZ; (c) the change in whole rock Mg# with stratigraphic height throughout the UUMZ (all data from *VanTongeren et al.* [2010]). In Figure 1a, all shades of blue in correspond to zones within the Rustenburg Layered Suite (teal = Upper Zone, blue = Main Zone; navy blue = Lower Zone; dark blue = Critical Zone). Purple = Dullstroom Formation; Green = Damwal Formation; Yellow = Kwaggasnek Formation; and Red = Schrikkloof Formation. Yellow dots and larger circles denote sampling locations within the map.

Layered mafic intrusions are fossilized shallow crustal magma chambers found worldwide and in many cases contain economic amounts of platinum group elements and chromite.

Among the layered mafic intrusions exposed today, the ~2.06 Ga Bushveld Complex located in the Kaapvaal craton is the largest. Within the Bushveld Complex, the mafic-ultramafic Rustenberg Layered Suite (RLS) was likely formed from four major pulses of magma, and the uppermost ~2.5 km of the 8–9 km thick intrusion are represented by the Upper and Upper Main Zones (UUMZ) (Figure 1). On the basis of major element, trace element, and isotopic geochemical trends, the rocks of the UUMZ are thought to reflect the crystallization products from the final pulse of magma into the chamber [e.g., *Kruger et al.*, 1987; *Tegner et al.*, 2006; *VanTongeren et al.*, 2010; *VanTongeren and Mathez*, 2013] with little to no volumetrically significant additional input of new magma or crustal contamination above this level. This makes the well-characterized RLS the ideal location in which to further investigate the evolution of Fe isotopes during fractional crystallization in a multiply saturated system (multiple phases on the liquidus at a given temperature) with and without magnetite.

Above a 3 m thick orthopyroxenite layer, the Pyroxenite Marker, the UUMZ is characterized by an evolving phase assemblage of pyroxene (px) + plagioclase (plag) → px + plag + magnetite (mgt) → px + plag + mgt + fayalitic olivine (ol) → px + plag + mgt + ol + apatite (ap). For the first ~1500 m, opx and cpx coexist, but opx disappears shortly after magnetite saturation. *VanTongeren et al.* [2010] showed that the cumulus mineral compositions and phase assemblages in the UUMZ evolved by fractional crystallization from a single parent magma composition from the Pyroxenite Marker to the roof of the intrusion (Figure 1 and supporting information Figure S1).

The lower ~500 m of the UUMZ is a two-pyroxene gabbro with approximately 40% pyroxene and 60% plagioclase. At ~2850 m cumulus magnetite joins the stratigraphy and is typically present as minor (2–10 modal %) disseminated grains throughout the gabbroic rocks. Below 2850 m, there is a small amount of intercumulus magnetite present. In addition, the Upper Zone is known for its 21 layers of nearly

monomineralic magnetitite. Magnetitite layers range in thickness from 10s of cm, to >3 m for the Main Magnetite Layer, however local variations in thickness do occur. For example, the uppermost magnetite layer (Seam 21) in the eastern Bushveld reaches up to 60 m thick in certain locations. Fayalitic olivine becomes a liquidus phase at ~3500 m, forming an initial troctolite horizon before the stratigraphy becomes dominated by ol-diorites for the remainder of the crystallization sequence. In this study, we report Fe isotope data from whole rocks and magnetite separates throughout the stratigraphy of the UUMZ in the eastern Bushveld Complex to investigate the effect of magmatic differentiation on the isotopic evolution of the magma in a well-characterized, large intrusion.

Considering the available published data on Fe isotope fractionation at relevant magmatic conditions, one would predict that whole rock isotopic compositions of samples near the bottom of the UUMZ (i.e., prior to magnetite saturation with abundant Fe^{2+}-rich phases) would be isotopically lighter than those near the roof. Assuming crystallizing phases are separated instantaneously from the melt, around the stratigraphic level of magnetite saturation, we would expect the whole rock Fe isotope composition to peak at its heaviest and become lighter stratigraphically upward. Deviations from, or consistency with, this hypothesized pattern will provide insight into the magmatic processes that formed the layered rocks of UUMZ.

2. Estimating Fe Isotope Evolution Throughout the UUMZ During Fractional Crystallization

We construct a simple model that incorporates the normative abundances of all cumulus phases throughout the UUMZ, their FeO contents, and their fractionation factors, in order to investigate the effect of fractional crystallization on the Fe isotope composition of the bulk rocks throughout the UUMZ. The Fe isotope composition of the UUMZ is likely controlled by the phase containing the largest proportion of the Fe in the rocks: magnetite. In addition, published fractionation factors imply a large fractionation of Fe isotopes between magnetite and melt. Each of the other Fe-bearing phases present (ol, opx, cpx, plag) will also have a varying effect. Therefore, it is reasonable to expect that the Fe isotope systematics of the UUMZ will reflect fractional crystallization, and accumulation.

Our model of the UUMZ assumes perfect fractional crystallization; i.e., a controlled amount of liquid crystallizes at each step (5% of the initial liquid present, not 5% of the liquid present at each step). The model stops at 15% liquid remaining, at which point the residual magma is erupted to the surface to form portions of the Rooiberg Group lavas and/or Rashoop Granophyres. This was proposed by *VanTongeren et al*. [2010] on the basis of MELTS phase equilibria and further supported by trace element equilibrium between the uppermost cumulates and the Rooiberg lavas [e.g. *VanTongeren and Mathez*, 2012]. Values incorporated into the model for percent liquid remaining are correlated to the stratigraphic height in the UUMZ according to the following relationship:

$$\text{Liquid remaining } (\%) = 15 + 100 \times (4625 - d) \div 2850 \quad (1)$$

where d represents the stratigraphic depth in meters above the Merensky Reef in the eastern Bushveld. The term 100*(4625 – d) is then divided by the original thickness of the UUMZ magma column prior to eruption. The Pyroxenite Marker defines the base of the UUMZ at 2200 m (100% liquid remaining). The roof of the UUMZ is at 4625 m (15% liquid remaining). The total original thickness of magma present in the UUMZ is 2850 m, which takes into account the total current UUMZ thickness of 2425 m plus the 425 m of magma estimated to be lost (15% of the original) [e.g., *VanTongeren et al*., 2010].

2.1. Modeling the Evolution of δ^{56}Fe

The isotopic composition of a system (i.e., whole rock) can be calculated from the sum of the isotopic values of each component (i.e., each mineral) weighted by their relative abundances. The fractionation of Fe isotopes throughout the UUMZ stratigraphy was modeled by the mass balance equations:

$$\delta^{56}Fe_{liquidY} = X_{liquid(Y-1)} \times \delta^{56}Fe_{liquid(Y-1)} - X_{WR(Y-1)} \times \delta^{56}Fe_{WR(Y-1)} \quad (2)$$

AGU Geochemistry, Geophysics, Geosystems 10.1002/2016GC006660

Table 1. Abbreviated Compilation of Model Inputs[a]

% Liquid Remaining	100	95	90	85	80	75	70	65	60	55	50	45	40	35	30	25	20	15
Equivalent strat. height	2202.5	2345	2487.5	2630	2772.5	2915	3057.5	3200	3342.5	3485	3627.5	3770	3912.5	4055	4197.5	4340	4482.5	4625
Projected modes																		
Plagioclase	0.53	0.53	0.53	0.53	0.53	0.53	0.53	0.53	0.53	0.53	0.53	0.53	0.53	0.53	0.53	0.53	0.53	0.53
Orthopyroxene	0.312	0.278	0.244	0.210	0.176	0.143	0.109	0.075	0.041	0.007	0	0	0	0	0	0	0	0
Clinopyroxene	0.158	0.192	0.226	0.260	0.294	0.327	0.361	0.395	0.429	0.245	0.240	0.227	0.215	0.203	0.190	0.178	0.166	0.153
Olivine	0	0	0	0	0	0	0	0	0	0.15	0.15	0.15	0.15	0.15	0.15	0.15	0.15	0.15
Magnetite	0	0	0	0	0.004	0.012	0.021	0.029	0.037	0.045	0.054	0.062	0.070	0.078	0.087	0.095	0.103	0.111
Ilmenite	0	0	0	0	0.002	0.006	0.010	0.014	0.018	0.023	0.027	0.031	0.035	0.039	0.043	0.047	0.051	0.055
Fe content of each phase (FeO phase/FeO WR)																		
Plagioclase	0.067	0.057	0.049	0.042	0.037	0.032	0.028	0.024	0.021	0.019	0.016	0.014	0.012	0.010	0.009	0.007	0.006	0.005
Orthopyroxene	2.315	2.228	2.158	2.101	2.053	2.013	1.978	1.948	1.921	1.898	1.877	1.858	1.841	1.826	1.812	1.799	1.788	1.777
Clinopyroxene	0.526	0.604	0.666	0.718	0.761	0.797	0.828	0.855	0.879	0.900	0.919	0.936	0.951	0.964	0.977	0.988	0.999	1.008
Olivine	0	0	0	0	0	0	0	0	0	2.665	2.713	2.756	2.794	2.829	2.861	2.890	2.917	2.941
Magnetite	0	0	0	0	7.783	7.192	6.685	6.245	5.859	5.518	5.215	4.943	4.698	4.476	4.275	4.090	3.921	3.765
Ilmenite	0	0	0	0	4.501	4.160	3.866	3.612	3.388	3.191	3.016	2.859	2.717	2.589	2.472	2.365	2.268	2.178
δ56Fe of each phase (calculated)																		
Liquid	0.168	0.165	0.154	0.144	0.135	0.126	0.116	0.106	0.096	0.086	0.074	0.063	0.052	0.042	0.033	0.025	0.018	0.012
Plagioclase	0.2	0.2	0.2	0.2	0.2	0.2	0.2	0.2	0.2	0.2	0.2	0.2	0.2	0.2	0.2	0.2	0.2	0.2
Orthopyroxene	0.060	0.054	0.041	0.027	0.014	0.001	−0.012	−0.027	−0.041	−0.057	−0.074	−0.091	−0.108	−0.125	−0.141	−0.156	−0.171	−0.185
Clinopyroxene	0.060	0.054	0.041	0.027	0.014	0.001	−0.012	−0.027	−0.041	−0.057	−0.074	−0.091	−0.108	−0.125	−0.141	−0.156	−0.171	−0.185
Olivine	0.125	0.121	0.109	0.097	0.087	0.076	0.064	0.053	0.040	0.028	0.013	−0.001	−0.015	−0.028	−0.041	−0.052	−0.063	−0.074
Magnetite	0.253	0.253	0.245	0.238	0.231	0.225	0.218	0.211	0.204	0.197	0.188	0.179	0.172	0.165	0.159	0.155	0.152	0.149
Ilmenite	0.125	0.121	0.109	0.097	0.087	0.076	0.065	0.053	0.042	0.030	0.016	0.003	−0.010	−0.022	−0.034	−0.044	−0.054	−0.062
Measured Data																		
Sample name	B07-009	B06-062	B06-064	B06-065	B06-067			B07-057	B06-020[b]	B07-061	B06-054	B06-042	B06-039	B06-029	B07-027	B06-037	B07-036	B07-041
Strat. height	2210	2325	2495	2620	2775			3122	3260	3425	3634	3741	3925	4083	4232	4305	4460	4590
% liquid equivalent	99.74	95.70	89.74	85.35	79.91			67.74	62.89	57.11	49.77	46.02	39.56	34.02	28.79	26.23	20.79	16.23
Modes from LSQR Matlab [*VanTongeren et al.*, 2010]																		
Plagioclase	0.45	0.37	0.54	0.56	0.49	NA	NA	0.58	0.49	0.84	0.79	0.44	0.46	0.46	0.54	0.55	0.46	0.42
Orthopyroxene	0.31	0.49	0.21	0.22	0.23	NA	NA	0.14	0.19	0.06	0.00	0.00	0.00	0.00	0.00	0.00	0.00	0.00
Clinopyroxene	0.22	0.13	0.25	0.21	0.26	NA	NA	0.16	0.19	0.01	0.09	0.29	0.30	0.10	0.05	0.06	0.16	0.20
Olivine	0.00	0.00	0.00	0.00	0.00	NA	NA	0.00	0.00	0.00	0.05	0.17	0.12	0.24	0.23	0.22	0.24	0.19
Magnetite	0.00	0.00	0.00	0.00	0.00	NA	NA	0.08	0.09	0.04	0.04	0.03	0.06	0.07	0.07	0.07	0.00	0.02
Ilmenite	0.00	0.00	0.00	0.00	0.00	NA	NA	0.02	0.01	0.02	0.02	0.04	0.04	0.04	0.04	0.04	0.05	0.04
Modeled whole rock Fe isotope composition based on observed modes and calculated liquid composition																		
Whole Rock δ56Fe	0.06	0.07	0.03	0.02	0.01	NA	NA	0.10	0.09	0.04	0.04	0.01	0.02	0.02	0.02	0.00	−0.07	−0.06

[a]NA—modes were not available for that sample. For a working version of the model with accompanying justification of all terms reiterated from the text, please see the supporting information.
[b]This is the mode of B06-021.

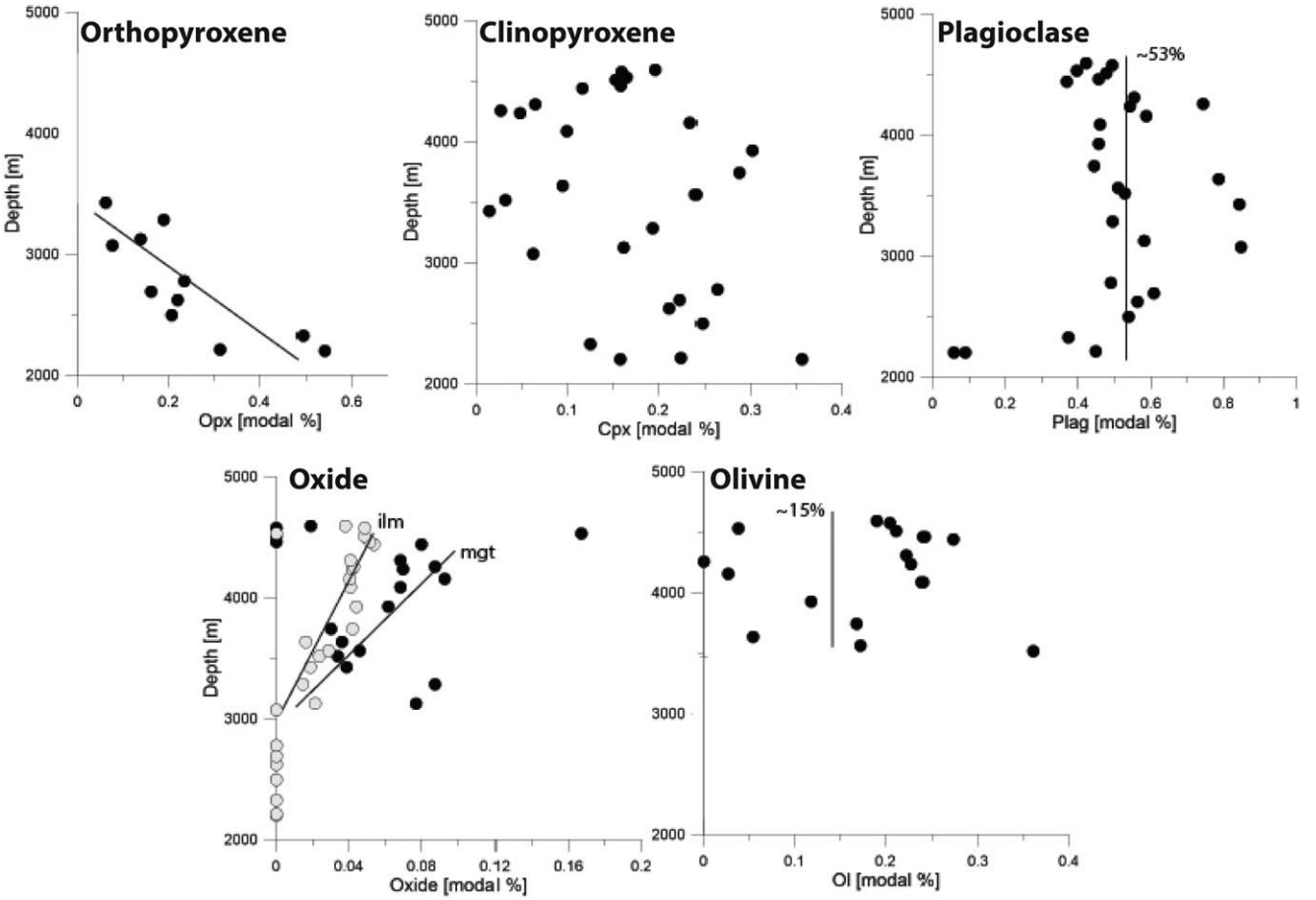

Figure 2. Normative abundances of constituent minerals with stratigraphic height. Lines indicate the trend of "projected modal abundances" used in the fractional crystallization model (see supporting information for details). Due to the lack of trend in the normative abundance of clinopyroxene with stratigraphic height, the projected normative abundance of clinopyroxene was calculated as Cpx [modal%] = 1 – Plag [modal%] – Opx [modal%] – Oxide [modal%] – Ol [modal%].

$$\delta^{56}Fe_{WR} = \delta^{56}Fe_{phase1} \times X_{phase1} \times \frac{FeO_{phase1}}{FeO_{WR}} + \delta^{56}Fe_{phase2} \times X_{phase2} \times \frac{FeO_{phase2}}{FeO_{WR}} + \ldots + \delta^{56}Fe_{phaseX} \times X_{phaseX} \times \frac{FeO_{phaseX}}{FeO_{WR}} \quad (3)$$

where Y is the current step within the evolution of the magma and Y − 1 represents the previous step. In equation (2), X_{liquid} is the proportion of liquid remaining and X_{WR} is the mass fraction of whole rock that is removed (i.e., crystallized) at each step. In equation (3), X represents the normalized modal abundance of an individual phase within the whole rock and FeO_{phase}/FeO_{WR} represents the fraction of FeO that the phase contributes to the whole rock value (Figure 3 and Table 1).

For each step, equations (2) and (3) require knowledge of (1) an estimate of the initial δ^{56}Fe of the parent melt; (2) the crystallizing phase assemblage and proportion of phases; and (3) the amount (Figure 3) and isotopic composition of Fe in each phase.

1. The starting δ^{56}Fe of the modeled liquid was fixed at 0.17‰ (Table 1). This value was chosen to match the observed $\delta^{56}Fe_{WR}$ value at the base of the UUMZ (see Results below), however, the initial $\delta^{56}Fe_{liquid}$ assumption has no bearing on the trends produced by the model.
2. Normative abundances of each phase are based on values reported by *VanTongeren et al.* [2010] (Figures 1 and 2, and Table 1), and all approximations of abundances from whole rock data were verified within 2–3 modal% by point counting of a representative thin section. Due to the presence of large (meters to tens of meters) and small (cm) scale modal layering in the UUMZ, the modal abundance of an individual hand-sample may not be representative of the liquidus proportions. To account for this in our modeling

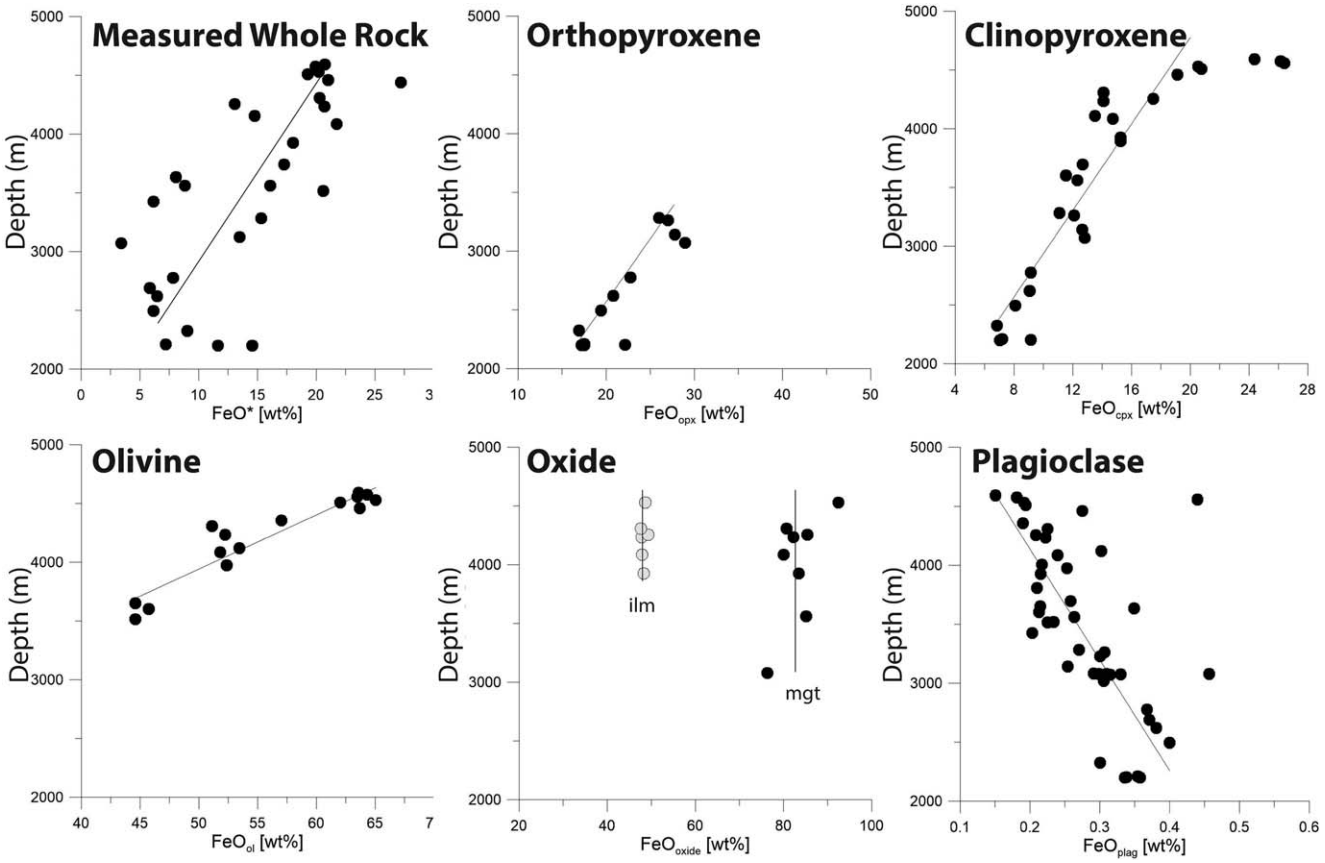

Figure 3. Observed FeO (wt.%) of whole rock and mineral phases with stratigraphic height. Lines indicate the compositional trend used in the fractional crystallization model.

of the liquid line of descent, we fit a line through all of the normative abundances from *VanTongeren et al.* [2010] with stratigraphic height (Figure 2). In the UUMZ, pyroxene modal abundance generally decreases with increasing stratigraphic height (from 50% at the base to 15% at the roof); above cumulus magnetite saturation, oxide modal abundance generally increases (from 2% to 15%); and above olivine saturation, its normative abundance remains relatively constant, at approximately 15% (although it varies between 0 and 35%; Figure 2). Based on this observation, the "projected" abundance calculated from the best-fit line at each stratigraphic height, and therefore each % liquid remaining step, was used in our liquid line of descent modeling (supporting information Table S1, "Step 1" of the working model).

The abundance of an individual mineral ($X_{mineral}$) was considered to be 0 until the stratigraphic height at which it appears as a cumulus phase (pyroxene: 2200 m and 100% liquid remaining; magnetite: ~2850 m and ~80% liquid remaining; olivine: ~3500 m and ~55% liquid remaining).

3. The FeO content of each phase was also incorporated in order to accurately portray the effect of each phase on the whole rock isotopic composition by compensating for mineral phases that are abundant (Figure 2) but do not contain much Fe (e.g., plagioclase) (Figure 3, details below).

The Fe isotope composition of each mineral phase was calculated or assigned based on published data. All fractionation factors ($\Delta^{56}Fe_{phaseA\text{-}phaseB}$) used in the model are from previously published field or laboratory-based studies and are calculated by incorporating T and converting to $\Delta^{56}Fe_{phaseA\text{-}phaseB}$ by the relationship: $\Delta^{57}Fe_{phaseA\text{-}phaseB}/1.5 = \Delta^{56}Fe_{phaseA\text{-}phaseB}$. The use of these fractionation factors also requires an assumption of equilibrium. The temperature-dependent equations for each cumulus Fe-bearing mineral are:

$$\Delta^{56}Fe_{pyroxene-melt} \leq -0.25 \times \left(\frac{10^6}{T^2}\right) \div 1.5 \quad [Sossi\ et\ al.,\ 2012]$$

$$\Delta^{56}Fe_{magnetite-melt} = 0.2 \times \left(\frac{10^6}{T^2}\right) \div 1.5 \quad [Sossi\ et\ al.,\ 2012]$$

$$\Delta^{56}Fe_{magnetite-fayalite} = 0.30 \times \left(\frac{10^6}{T^2}\right) \div 1.5 \quad [Shahar\ et\ al.,\ 2008]$$

The $\Delta^{56}Fe_{pyroxene\text{-}melt}$ and $\Delta^{56}Fe_{magnetite\text{-}melt}$ equations are derived from measurements of samples from the Red Hill Intrusion, described in section 1, which is a sill containing dolerite and granophyre that was injected in a single event and evolved as a closed system [*Sossi et al.*, 2012, section 1]. $\Delta^{56}Fe_{fayalite\text{-}magnetite}$ is based on data obtained from a series of experiments over a range in temperatures performed by *Shahar et al.* [2008] and is consistent with the study of *Roskosz et al.* [2015]. The experimental approach utilized the three-isotope method in which a "spike" of one isotope of Fe is added to one experimental phase and time-series runs are performed. In this way, equilibrium can be graphically projected if not fully obtained. These equations are the only mineral-melt fractionation factors available in the literature, to our knowledge, which are applicable for the T range and composition of the UUMZ. Clinopyroxene and orthopyroxene compositions were calculated by using the same fractionation factor since Fe isotope fractionation is not expected to differ [*Roskosz et al.*, 2015], while ilmenite was treated like fayalite, consistent with the findings of *Sossi and O'Neill* [2017]. Magnetite and olivine were not included in the model until the height at which they appear as a cumulus phase (Figures 1 and 2, and Table 1), even though small amounts of intercumulus magnetite and olivine occur in the rocks of the UUMZ below these levels.

Due to the temperature dependence of isotope fractionation, we calculate crystallization temperatures by utilizing results from the T_{REE} thermometer of *Sun et al.* [2013] and *Liang et al.* [2013], who observe a linear change in temperature from ~1250°C at 2200 m to ~1050°C at 3500 m in the UUMZ. Above ~3500 m in the stratigraphy, the REE thermometer is no longer calibrated for the compositional range. However, due to the linearity of the thermometer below 3500 m, we are able to calculate the temperatures for the stratigraphy from 3500 to 4625 m by assuming the same slope in temperature versus stratigraphic height. Over the course of the entire UUMZ stratigraphy, the crystallization temperature in our model decreases by ~15°C per 5% decrease in percent liquid remaining (i.e., at each model step). Using the two-pyroxene thermometer or the QUILF program would be insufficient here since both approaches would only allow for the determination of closure temperature of the system. Since layered intrusions are generally expected to cool slowly, those temperatures would likely be reset considerably.

Last, since the whole rocks contain a normative abundance of plagioclase of up to 86% (Figure 2), it was incorporated into the model despite this phase's low Fe content. Little work has been done thus far to constrain the Fe isotopic composition of plagioclase in terrestrial magmatic systems, but *Wang* [2013] found that lunar regolith plagioclase has a δ^{56}Fe of 0.15–0.30‰. Thus, we fixed the $\delta^{56}Fe_{plagioclase}$ value at 0.20‰. However, it is important to note that plagioclase contributes such a small amount of FeO to the system that despite its abundance, it does not significantly influence the model regardless of its Fe isotopic value.

For a working version of the model with annotations that reiterate the justification of parameters described here, please consult the supporting information, Table S1.

2.2. Model Results

The results of our fractional crystallization model for the UUMZ are shown in Figure 3. Our model reveals three important trends: (1) despite the positive mineral-melt fractionation factor for magnetite ($\Delta^{56}Fe_{mgt\text{-}melt}$ = ~0.2 * $10^6/T^2$/1.5) [*Sossi et al.*, 2012], the low abundance of magnetite relative to pyroxene and olivine in the UUMZ samples buffers the effect of magnetite crystallization on the evolution of δ^{56}Fe in the liquid. Consequently, our model predicts only a subtle change in the δ^{56}Fe of the liquid from 0.17‰ to 0‰ through the whole UUMZ and no major shift in slope after magnetite or olivine saturation (Figure 4). (2) The model predicts an overall decrease in the $\delta^{56}Fe_{WR}$ of about 0.11‰. This is likely due to the decreasing proportion of FeO contributed to the whole rock by magnetite relative to the isotopically lighter phases pyroxene and olivine in the cumulus assemblage (Figure 3). The amount of FeO in the whole rock that is contributed by pyroxene and olivine increases with stratigraphic height while the proportion of FeO in the whole rock from magnetite remains constant. (3) The model also predicts no significant change in $\delta^{56}Fe_{mgt}$ with stratigraphic height, varying just 0.08‰ throughout the UUMZ (supporting information, Table S1).

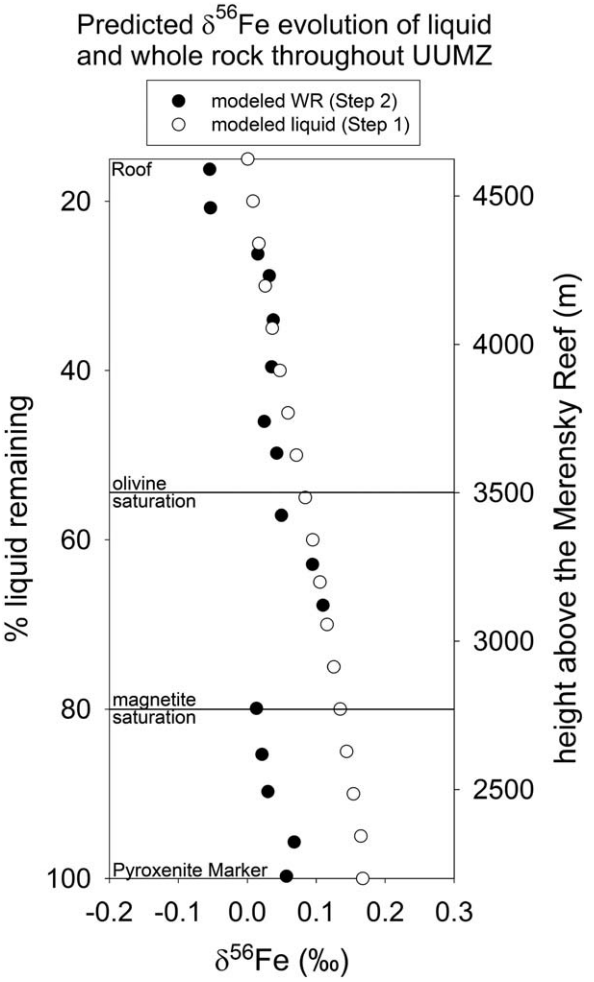

Figure 4. Predicted evolution of the Fe isotope composition of the liquid and whole rock (WR) based only on the projected and observed normative abundances, respectively (see "Step 1" for the liquid and "Step 2" for the whole rock in the supporting information). The model incorporates published fractionation factors (pyroxene, magnetite, olivine), available published $\delta^{56}Fe_{plagioclase}$ data, calculated crystallization temperatures over the stratigraphy, and the Fe content of each phase. The % liquid remaining is calculated for each stratigraphic height assuming 15% magma loss from the UUMZ to form some portion of the Rooiberg Group lavas and/or Rashoop Granophyres [e.g., *VanTongeren et al*., 2010; *Mathez et al*., 2013]. Approximate saturation levels for magnetite and fayalite are noted with solid black lines at about 80% and 55% liquid remaining, respectively.

The lack of change in δ^{56}Fe predicted by the fractional crystallization model is somewhat surprising given previously published fractionation factors for single minerals [e.g., *Schuessler et al*., 2007; *Shahar et al*., 2008; *Sossi et al*. 2012], which predict a large crystal-liquid fractionation. In order to test our model results, we present data on δ^{56}Fe for whole rock and magnetite mineral separates in the UUMZ of the Bushveld Complex.

3. Sampling and Analytical Methods

3.1. Sampling Details

Samples were collected from exposed sections of the eastern limb of the RLS and are the same as those analyzed in the studies of *VanTongeren et al*. [2010], *VanTongeren and Mathez* [2012], and *VanTongeren and Mathez* [2013] (Figure 1). We analyzed 22 whole rock samples, measuring the Fe isotopic composition of the UUMZ approximately every 100 m within the ~2.5 km thick section (Figure 1). Above cumulus magnetite saturation, magnetite is the dominant control on the Fe concentration in the whole rock in that it contributes more FeO than any other Fe-bearing phase (Figure 3). Accordingly, magnetite separates were analyzed from each sample where available (20 of 22 samples) in order to determine their control on the Fe isotopic composition of the whole rocks.

3.2. Sample Preparation

To prepare the samples for isotopic analysis, magnetite was first separated by hand magnet and subsequently picked under a binocular microscope at 30x magnification. Only magnetite grains without visible impurities were used. About 5–10 mg of whole rock samples was measured out so that no more than ~500 μg of Fe was processed through the columns later. Magnetite samples were measured out to weigh 0.5–1 mg. Crushed whole rock samples were first digested in a solution of HF and HNO_3 on a hot plate and dried down. Magnetite and whole rock samples were digested on a hotplate in *aqua regia*, dried down, and digested and dried again in 8 *N* HCl prior to column chemistry. The 1 mL columns were filled with Biorad AG1-X8 ion exchange resin, which was conditioned prior to samples being loaded. First, the column reservoir was filled with 8 *M* HNO_3, followed by 1 full reservoir of H_2O, 1 full reservoir of 0.1 *N* HCl, and finally 2 mL 8 *N* HCl. The sample was dissolved again on the hotplate in 0.2 mL 8 *N* HCl for loading. Next, the resin was rinsed four times by using 0.5 mL of 8 *N* HCl. Then, to elute the Fe 0.5 mL of 8 *N* HNO_3 was introduced, and then 1 mL of 0.5 *N* HCl was introduced twice. Next, 0.5 mL of H_2O, 1 mL 8 *N* HNO_3, and then 0.5 mL of H_2O were used in succession to elute the rest of the Fe. *Zambardi et al*. [2014] used the same column chromatography method and demonstrated that Ca, Na, Al, and Mg were eluted prior to Fe and did not linger in the columns. They also checked that Fe was not being eluted early with the matrix and

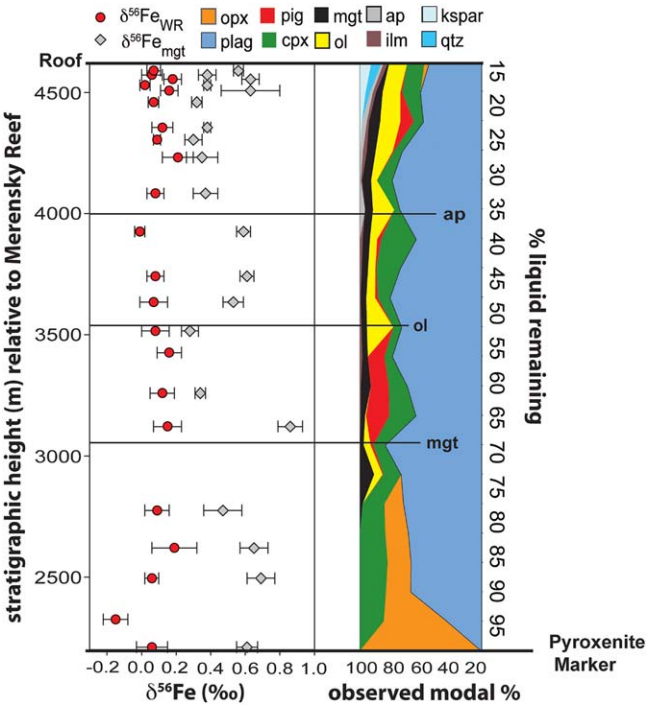

Figure 5. Measured Fe isotope compositions of whole rock (circles) and magnetite (diamonds) samples plotted at stratigraphic height relative to the Merensky Reef. These data are compared to the normative abundances of phases from the base of the UUMZ (Pyroxenite Marker at 2200 m) to the roof (4625 m). All normative abundance approximations from whole rock data were verified within 2–3 modal % by point counting of a representative thin section and observed modal % values were calculated by least squares by incorporating measured geochemical data (modified from *VanTongeren et al.* [2010]). Error bars are 2σ. Ap—apatite saturation; ol—olivine saturation; mgt—magnetite saturation.

routinely checked that the column yields were ~99%. Zinc may also be of concern when using this elution scheme for digested whole rock samples, however, *Millet et al.* [2012] demonstrated that Zn only interferes with Fe during analysis by multicollector inductively coupled plasma mass spectrometer (MC-ICP-MS) when the two elements are present in the same concentration. In these Bushveld samples, Zn concentrations vary between 50 and 180 ppm while Fe concentrations are never below 5 wt.%.

Samples were then dried down and redissolved in 20 μL of concentrated HNO_3 before being dried down one last time before analysis. All acids used were subboiling distilled and all water used was ultrapure. During each session of column chromatography, we produced 1 blank sample to monitor for potential environmental contamination. The Fe blank was insignificant (<0.1%) relative to the amount of Fe loaded on the column.

3.3. Analytical Details

After performing the column chromatography, samples were dissolved in

Table 2. δ^{56}Fe Values From Whole Rock and Magnetite Analyses With Associated 2σ and Lithology of the Accompanying Unit

Stratigraphic Position Relative to the Merensky Reef (m)	Sample Number	Latitude (S)[a]	Longitude (E)[a]	Equivalent % Liquid Remaining	$\delta^{56}Fe_{WR}$(‰)	2σ	$\delta^{56}Fe_{magnetite}$ (‰)[b]	2σ[b]	Lithology
2210	B07-009	24°51.778′	29°58.114′	99.74	0.06	0.09	0.61	0.06	Gabbro
2325	B06-062	24°51.778′	30°01.770′	95.70	−0.15	0.07	NA	NA	Gabbro
2495	B06-064	24°51.851′	30°01.842′	89.74	0.06	0.04	0.69	0.08	Gabbro
2620	B06-065	24°51.858′	30°01.565′	85.35	0.19	0.13	0.65	0.08	Gabbro
2775	B06-067	24°51.917′	30°01.398′	79.91	0.09	0.07	0.47	0.11	Gabbro
3122	B07-057	24°48.985′	29°58.275′	67.74	0.15	0.08	0.86	0.07	Gabbro
3260	B06-020	24°48.974′	29°58.149′	62.89	0.12	0.07	0.34	0.03	Gabbro
3425	B07-061	24°48.914′	29°57.798′	57.11	0.16	0.07	NA	NA	Anorthosite
3515	B06-024	24°48.910′	29°57.711′	53.95	0.08	0.08	0.28	0.05	Troctolite
3634	B06-054	24° 48.763′	29°57.186′	49.77	0.07	0.08	0.53	0.06	Gabbro
3741	B06-042	24°48.776′	29°57.036′	46.02	0.08	0.05	0.61	0.04	Gabbro
3925	B06-039	24°48.857′	29°56.833′	39.56	−0.01	0.03	0.59	0.04	Gabbro
4083	B06-029	24°48.895′	29°56.650′	34.02	0.08	0.05	0.37	0.07	Troctolite
4232	B07-027	24°49.072′	29°56.433′	28.79	0.21	0.09	0.35	0.09	Diorite
4305	B06-037	24°48.747′	29°56.407′	26.23	0.09	0.02	0.30	0.05	Diorite
4355	B06-055	24°51.874′	29°54.756′	24.47	0.12	0.06	0.38	0.02	Diorite
4460	B07-036	24°51.845′	29°54.607′	20.79	0.07	0.03	0.32	0.03	Diorite
4508	B07-037	24°51.827′	29°54.550′	19.11	0.16	0.05	0.63	0.17	diorite
4530	B07-038	24°51.823′	29°54.519′	18.33	0.02	0.06	0.38	0.02	Diorite
4555	B07-039	24°51.800′	29°54.488′	17.46	0.18	0.04	0.63	0.05	Diorite
4573	B07-040	24°51.794′	29°54.465′	16.82	0.06	0.06	0.38	0.05	Diorite
4590	B07-041	24°51.829′	29°54.430′	16.23	0.07	0.03	0.56	0.03	Diorite

[a]GPS coordinates form *VanTongeren et al.* [2010], *VanTongeren and Mathez* [2012], and *VanTongeren and Mathez* [2013].
[b]NA indicates that not enough pure magnetite could be separated from the sample for Fe isotope analysis.

2% HNO_3 for introduction to the mass spectrometer. Stable Fe isotope analyses were performed on whole rock ($\delta^{56}Fe_{WR}$) and magnetite ($\delta^{56}Fe_{mgt}$) samples by using a Nu Plasma HR MC-ICP-MS at the University of Illinois, Urbana-Champaign. Mass resolution was >6000 and samples were run in dry plasma mode with a desolvating nebulizer system. All standard and sample solutions were run at concentrations of ~1 ppm. We employed the ^{57}Fe-^{58}Fe double-spike method of *Millet et al*. [2012] by adding 0.5 ppm of well-characterized spike solution containing a known composition of ^{57}Fe and ^{58}Fe to all measured samples and standards, including those used to bracket sample measurements. The double spike deconvolution was performed online during the analytical method, wherein the precise isotopic composition of the double spike solution was taken into account. It entails an online iteration that subtracts from the measured values the contributions from the double spike solution and calculates mass bias with convergence within 10 calculation cycles. The IRMM-014 (Institute of Reference Materials and Measurements standard number 014) bracketing standard was run between every sample analysis and secondary standards (BCR-2, UI-Fe) were run as every fourth sample. This standard-sample bracketing method is widely used to correct for instrumental mass bias and improve data precision. To correct for interferences with Ni on ^{58}Fe and Cr on ^{54}Fe, each sample and standard analysis included measurements of these two elements, and the data were used to adjust the analyzed Fe values accordingly. The average ratio ($\pm 2\sigma$) of 52/54 was 0.0001 ($\pm$0.002) and the average ratio of 60/58 was 0.00006 ($\pm$0.0001).

4 Results

Data are reported in Table 2 and Figure 5 in the conventional delta notation, following the equation:

$$\delta^{56}Fe_{sample}\ (‰) = \left[\left(\frac{^{56}Fe}{^{56}Fe} \right)_{sample} \div \left(\frac{^{56}Fe}{^{56}Fe} \right)_{IRMM-014} - 1 \right] \times 1000 \quad (4)$$

Each unknown sample and standard measurement included 2–3 repeated analyses. USGS rock powder standard BCR-2 was also processed alongside unknown samples. BCR-2 and in-house standard UI-Fe were analyzed throughout each session to monitor accuracy and instrumental drift. The precision reported is given based on the 2SD of 2–3 repeat analyses, and reported as 0.03‰ if there was no variation between the analyses (i.e., $2\sigma = 0.00‰$). USGS rock powder standard BCR-2 gives 0.06 $\pm$0.09‰ (average over one 5 day analytical session; n = 9), which is within error of other studies [*Dauphas et al*., 2009; *Wombacher et al*., 2009; *Craddock and Dauphas*, 2011; *Huang et al*., 2010; *Sossi et al*., 2012]. The in-house standard UI-Fe gives $\delta^{56}Fe = 0.71‰ \pm 0.04‰$ (2SD, n = 8 throughout the same 5 day session).

We observe little variability within a tight range of $\delta^{56}Fe_{WR}$ values throughout the UUMZ; $\delta^{56}Fe_{WR}$ ($\pm 2\sigma$) ranges from $-0.01 \pm 0.03‰$ to $0.21 \pm 0.09‰$ ($\delta^{56}Fe_{WR}$ average ~0.10 $\pm$0.09‰, excluding isotopically light outlier B06-062, $\delta^{56}Fe_{WR} = -0.15 \pm 0.07‰$). There is no correlation with stratigraphic height and therefore magma evolution within the UUMZ (Figure 5 and Table 2). Measured $\delta^{56}Fe_{mgt}$ ($\pm 2\sigma$) are consistently isotopically heavier than their whole rock counterparts, an expected pattern based on experimental data [*Shahar et al*., 2008] and measurements of natural samples [e.g., *Heimann et al*., 2008]. In general, however, the stratigraphic variations in UUMZ magnetite are also unsystematic ($\delta^{56}Fe_{mgt} = 0.28 \pm 0.05‰$ to $0.86 \pm 0.07‰$; average = $0.48 \pm 0.16‰$) (Figure 5).

5. Discussion

5.1. The Effect of Fractional Crystallization on Fe Isotope Evolution

The observed absence of significant variation or a systematic trend in the Fe isotope composition of the UUMZ whole rock samples is consistent with our model (Figure 6), based on calculated parameters rather than measured ones. Our simple model mimics the overall variation observed in the measured Fe isotope composition of the UUMZ, particularly between ~80 and 30% liquid remaining, and therefore demonstrates that fractional crystallization plays an important role in the Fe isotope evolution of the UUMZ. Because the calculations of the predicted $\delta^{56}Fe_{WR}$ values are principally controlled by the abundance of individual Fe-bearing phases, each of which prefers a certain isotope, oxidation state of Fe, or coordination, the whole rock Fe isotope composition appears to be buffered by the changing Fe-bearing mineral assemblage. This

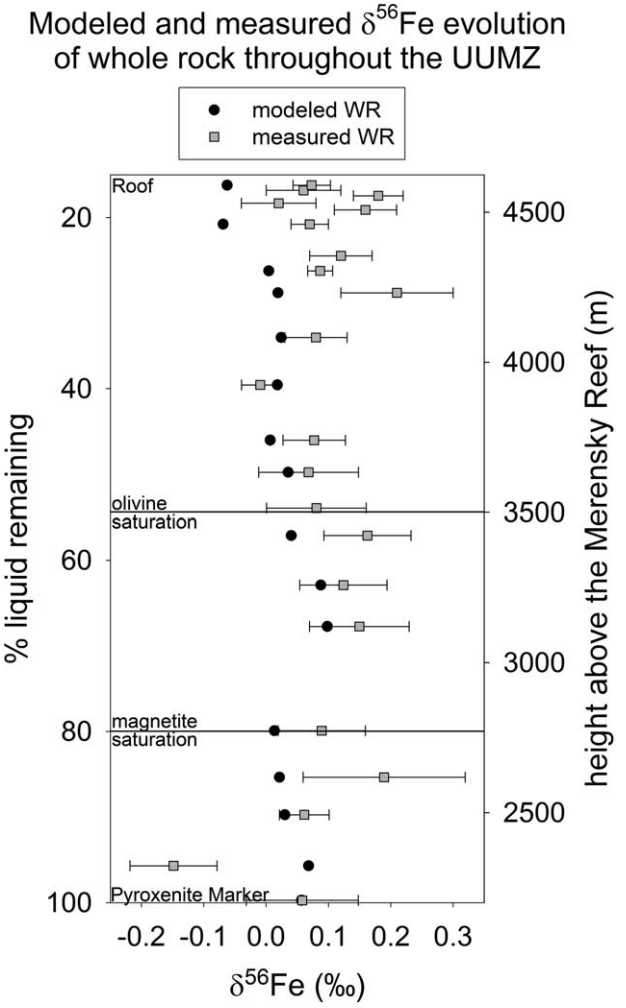

Figure 6. Comparison of the modeled evolution of the Fe isotope composition of the whole rock (WR) predicted solely from fractional crystallization (see "Step 2" in the supporting information) and the measured WR values (error bars are 2σ).

agrees with previous work, such as *Sossi et al.* [2012]. As we observe in the measured values, we predict a tight range and unsystematic variability in the overall trend throughout the stratigraphy (Figure 6).

In the uppermost portion of the stratigraphy (above 30% liquid remaining, ~4000 m above the Merensky Reef), the modeled and measured whole rock values diverge more, with the measured δ^{56}Fe values behaving quite erratically. This may be due to the fact that processes other than fractional crystallization play a key role in the formation of these rocks.

5.1.1. Comparison of Modeled and Measured δ^{56}Fe

The simplified fractional crystallization model for Fe isotopes (section 2) predicts that values for δ^{56}Fe in the whole rock and liquid would not change significantly with stratigraphic height in the UUMZ using the observed normative abundances of mineral phases. Modeled whole rock values are consistently lighter than measured whole rock in the UUMZ, with the exception of one sample prior to magnetite crystallization. Although we did not expect for our model to identically match the measured values, the differences between the predicted Fe isotope values and measured whole rock data may be a result of several factors.

First, the presence of an unknown amount of trapped melt in the whole rock samples could result in values higher or lower than model, depending on the relative proportions of cumulus pyroxene and magnetite in the whole rock. If the melt is indeed isotopically heavier than the whole rock as our model predicts, this could explain why our measured δ^{56}Fe values are more positive than the modeled ones. While there is currently no observed evidence of trapped melt in the samples analyzed, perhaps the Fe isotope data provides an indication.

We should also consider the model calculations themselves, which can provide insight into the measured values. Importantly, the fractionation factors were calculated from previously published experimental and natural samples, which may have crystallized under conditions different from those of the UUMZ. They also require an assumption of equilibrium. While there are published beta factors for some of the phases (which agree with the magnetite fractionation factor in our model) [*Roskosz et al.*, 2015], the paucity of these data at relevant conditions for every considered phase (ol, opx, cpx, mgt, ilm, melt, *and* plag) hindered the attempt to use these more recent data in the model. This may also be the case for the set isotopic value of plagioclase; however, the value does not significantly influence the model.

Another important aspect to note is that our modeled liquid, upon which our modeled whole rock relies, is based on *trends* in normative abundances with increasing stratigraphic height. This was done to compensate for the layered nature of the intrusion today. On the other hand, the calculated whole rock is based upon the normative abundances themselves. This projection of modes used in the calculation of the liquid may cause some smoothing of the modeled results that are not reflected in the measured data.

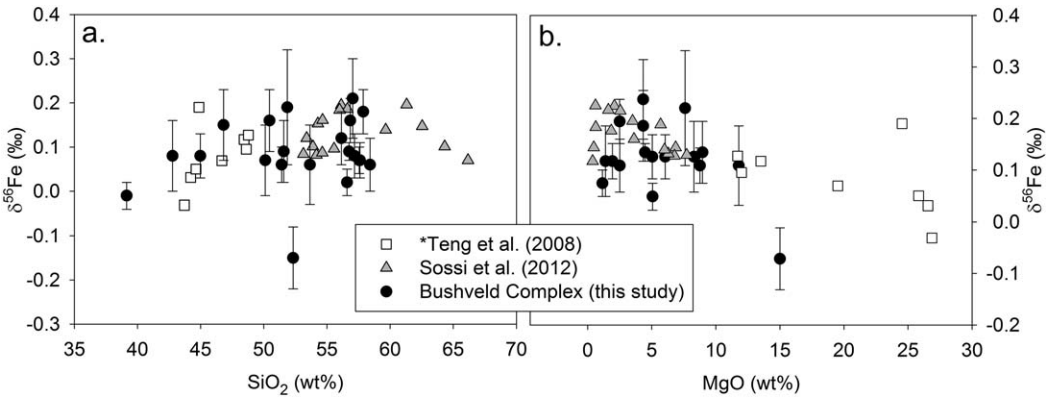

Figure 7. Whole rock Bushveld Complex δ^{56}Fe values (black circles, error bars are 2σ) from this study plotted versus (a) whole rock SiO_2 content and (b) MgO content with other published studies on igneous whole rocks that evolved from a single event closed to O_2 gain/loss. The isotopic range is consistent between the studies, and additional scatter within the Bushveld data is likely due to its layered nature. White squares – Kilauea Iki, Hawaii, USA [*Teng et al*., 2008]; gray triangles – Red Hill Intrusion, Tasmania [*Sossi et al*., 2012]. *Only *Teng et al*. samples with MgO content >7 wt.% were plotted, since these data are thought to reflect fractional crystallization processes.

Processes that occurred during or after the cooling of the intrusion may also have influenced the measured values. For example, diffusion of Fe at subsolidus conditions could alter the δ^{56}Fe values of individual minerals, and in the case of oxides this effect may be unequal [*Dziony et al*., 2014]. *Chen et al*. [2014] proposed this hypothesis to explain the discrepancy in the δ^{56}Fe values measured in magnetite and ilmenite collected from the Baima layered intrusion, China, where olivine and pyroxene were apparently unaltered by reequilibration of Fe isotopes. Therefore, our magnetite samples might be isotopically heavier than they were during crystallization, and this may also explain the erratic nature of the data (Figures 5 and 6). However, it is important to note that subsolidus reequilibration may occur to affect the δ^{56}Fe of individual phases but mobility of Fe is low, meaning that the whole rock faithfully records its magmatic signature. A major conclusion from previous Fe isotope studies is that whole rock compositions show systematic changes with index of differentiation and are thus best suited to understanding differentiation processes [*Poitrasson*, 2006].

Notably, the top portion (>4000 m above the MR, <35% liquid remaining) of the analyzed stratigraphy displays scattered measured values not mirrored by our estimations (Figure 6). *VanTongeren and Mathez* [2012] proposed that the uppermost 625 m of the Upper Zone underwent large-scale silicate liquid immiscibility, and the study of *Fischer et al*. [2016] identified the presence of both Fe-rich and Si-rich melt inclusions trapped in apatite grains within the Upper Zone. Our data within the potential liquid immiscibility portion do follow markedly different trends than the data below it (Figure 5). There currently exists no published fractionation factor to describe Fe isotope behavior between Fe-rich and Si-rich immiscible melts, but previous work does predict a measurable fractionation of Fe isotopes between the two melts.

Zhu et al. [2015] performed calculations based on mass diffusion that predict an enrichment of isotopically heavy Fe in the Si-rich melt relative to the bulk Fe-melt from which it formed. This is consistent with the work of *Dauphas et al*. [2014], although their conclusion is based on a different mechanism; they observe an increase in the force constants of Fe bonds in silicate glasses with SiO_2 content accompanying enrichment in isotopically heavy Fe. However, the fractionation of Fe isotopes between two such melts is quite complex and may also be controlled by factors including the growth rate of the immiscible melt, the concentration of SiO_2 and Fe in each melt, and Fe diffusivity. It is also likely that there is an unknown degree of isotopic reequilibrium between the two melts, which would attenuate the relative differences in δ^{56}Fe caused by liquid immiscibility. We cannot tell at this time whether the more Si-rich samples above 4000 m are isotopically heavier with respect to Fe isotopes due to liquid immiscibility or the fact that they are more evolved.

5.2. Measured $\delta^{56}Fe_{mgt}$ and Potential Implications for the Formation of the UUMZ Magnetitite Layers

One of the most well-known aspects of the Upper Zone of the Bushveld Complex is the presence of over 20 layers of nearly monomineralic magnetite [*Molyneux*, 1974] (supporting information Figure S2). Proposed hypotheses for the origin of these layers include gravitational settling [e.g., *Cawthorn and Ashwal*, 2009], periodic changes in fO_2 [e.g., *Klemm et al*., 1982; *Reynolds*, 1985] possibly due to new pulses of magma

added to the resident magma chamber [e.g., *Irvine and Sharpe*, 1986], pressure fluctuations [*Cawthorn and McCarthy*, 1980], and silicate liquid immiscibility [e.g., *Scoon and Mitchell*, 1994; *Harney and von Gruenewaldt*, 1995]. There is no recorded change in fO_2 in the UUMZ rocks analyzed here [c.f. *VanTongeren and Mathez*, 2012], and there is no change in the geochemical characteristics (isotopes, major and trace elements) above and below magnetite layers [c.f. *Cawthorn and Ashwal*, 2009] that would indicate formation due to new pulses of magma. Evidence for large-scale silicate liquid immiscibility exists in the diorites at the top of the UUMZ [*VanTongeren and Mathez*, 2012]; however, there is no such evidence available from the lower portions of the UUMZ, which also contain abundant magnetite layers.

Our measured $\delta^{56}Fe_{mgt}$ values are significantly but inconsistently isotopically heavier than the measured $\delta^{56}Fe_{WR}$ values. Comparably high $\delta^{56}Fe_{mgt}$ have also been reported in the Skaergaard [*Dziony et al*., 2014]. Above and below the magnetitite layers, the measured Fe isotope composition of the magnetite separates and corresponding whole rock samples do not markedly change. The lack of change in $\delta^{56}Fe_{mgt}$ and $\delta^{56}Fe_{WR}$ above and below magnetite layers in the UUMZ (supporting information Figure S2) suggests that the formation of these horizons is likely due to gravitational settling of magnetite as a result of normal fractional crystallization, consistent with the conclusions of *Cawthorn and Ashwal* [2009]. However, with the information currently available, further speculation about the formation of these layers is not possible.

5.3. Comparison of the Fe Isotope Systematics of the Bushveld With Other Single-Event Igneous Systems With Evidence of Fractional Crystallization

δ^{56}Fe values of whole rock samples from the UUMZ are consistent with previous studies of mafic or low silica intrusive igneous rocks (Figure 7). *Sossi et al*. [2012] measured the δ^{56}Fe composition of 16 whole rock and 6 magnetite-pyroxene pairs from the ~420 m thick Red Hill sill, Tasmania. This single injection of tholeiitic magma underwent fractional crystallization in a closed system, similar to the UUMZ albeit on a significantly smaller scale. They report increasing $\delta^{56}Fe_{WR}$ with decreasing whole rock MgO wt.% until magnetite saturation (Figure 7b), and attributed this to the effects of fractional crystallization of Fe-bearing phases on the $Fe^{3+}/\Sigma Fe$ of the melt. *Teng et al*. [2008] report a similar range in MgO wt.% versus Fe isotope composition of whole rocks from Kilauea Iki, Hawaii, in that δ^{56}Fe increases with decreasing MgO. Sossi et al. suggested that systems open to O_2 (i.e., buffered at a specific fO_2) would not record significant changes in $\delta^{56}Fe_{WR}$ until late in their crystallization history (i.e., higher SiO_2), whereas those closed to O_2 (e.g., Red Hill, Kilauea Iki) should display increasing $\delta^{56}Fe_{WR}$ throughout the stratigraphy (Figure 7b). Aside from differences in scale and layering, fayalite disappears as a cumulus phase after magnetite saturation in the Red Hill sill while fayalite cocrystallizes with magnetite throughout much of the top ~2 km of the Bushveld. Throughout the UUMZ, magnetite-ilmenite pairs record equilibrium fO_2 values near FMQ-1 [e.g., *VanTongeren and Mathez*, 2012], which is likely buffered by the presence of both fayalite and magnetite. Thus, the lack of systematic changes in fO_2 and $\delta^{56}Fe_{WR}$ in the UUMZ is consistent with the hypothesis of *Sossi et al*. [2012].

5.4. Comparison to the Baima Mafic Layered Intrusion

In the most comprehensive study of Fe isotope fractionation in layered mafic intrusions to date, *Chen et al*. [2014] provide δ^{56}Fe data for whole rock, olivine, pyroxene, magnetite, ilmenite mineral separates throughout the stratigraphy of the Baima Intrusion, China. They observed little change in $\delta^{56}Fe_{WR}$ with increasing stratigraphic height, but they noticed a distinctive trend of increasing magnetite δ^{56}Fe values with height. To a first order, the increase in magnetite δ^{56}Fe appears to be the opposite of that observed in our study (the $\delta^{56}Fe_{mgt}$ composition of samples near magnetite saturation is higher than the $\delta^{56}Fe_{mgt}$ composition of samples in the uppermost portion of the UUMZ). However, two important points must be considered: (1) The Baima Intrusion is unique in that the Basal and Lower Zones are dominated by Fe-Ti oxides, constituting up to 55 modal % of the rocks. The abundance of Fe-Ti oxides, and the ratio of magnetite/ilmenite, *decreases* with increasing stratigraphic height, which is opposite to what is observed in the UUMZ; (2) the Baima Intrusion received multiple pulses of magma throughout its crystallization history, and may not be a reliable record of closed system processes.

5.5. The Potential Effect of Ilmenite

Comparison with the Baima Intrusion also highlights the potential effect of subsolidus reequilibration between magnetite and coexisting Fe-bearing minerals (in particular ilmenite), which may contribute to the observed differences between the Baima and the UUMZ as well as the scatter in the measured δ^{56}Fe values

at the top of the stratigraphy (Figures 5 and 6). *Chen et al.* [2014] observed that the extent to which magnetite and ilmenite exchange chemically depends on their relative abundances within the rock. And in some cases, the magnetite likely retained its original δ^{56}Fe composition. On the other hand, the majority of the other Fe-bearing minerals that were analyzed (ol, cpx) had mantle-like Fe isotope compositions, interpreted to be largely unaffected by subsolidus reequilibration. *Dziony et al.* [2014] studied in detail Fe isotopic differences between coexisting magnetite and ilmenite in a variety of settings, including variable lithology from seafloor drill core (IODP hole 1256D, East Pacific Rise), massive hydrothermal deposits from the Mid-Atlantic Ridge, and gabbros from the Skaergaard Intrusion Middle Zone. In addition to varying differences between the two oxides in each setting, *Dziony et al.* also observed variations in $\delta^{56}Fe_{mgt}$ within individual grains, which has been demonstrated in other studies as well. Although it is important to point out that many of their samples had experienced extensive subsolidus fluid-rock interaction that likely modified the Fe isotope ratios, in general, magnetite was isotopically heavier than ilmenite. This is also consistent with the experimental work of *Sossi and O'Neill* [2017]. No correlation between the measured Fe isotope values of UUMZ whole rock and magnetite and the normative abundances of each of the oxides exists, however, we cannot rule out the accidental inclusion of a small amount of ilmenite in our magnetite fraction. Considering the information available for our UUMZ samples, disentangling the potential effect of ilmenite is not straightforward at this time.

6. Conclusions

We provide the first δ^{56}Fe data for whole rock and magnetite separates throughout the sequence of the UUMZ of the Bushveld Complex layered intrusion, the trends of which are consistent with a simple model based solely on fractional crystallization. Our model incorporates the normative abundances and FeO content of each Fe-bearing phase throughout the stratigraphy as well as published fractionation factors and calculated temperature changes. We predict no significant change in δ^{56}Fe in the whole rock or liquid during fractional crystallization of the multiply-saturated UUMZ. Measured $\delta^{56}Fe_{WR}$ values confirm this result, and do not change systematically with stratigraphic height, but do display slight variability that corresponds to changes in pyroxene, magnetite, and olivine normative abundance. Our data demonstrate two important points:

1. While crystallization of a single mineral phase will have an effect on the Fe isotopic evolution of the liquid, the overall effect of fractional crystallization of a multiply-saturated (i.e., buffered) nominally anhydrous Fe-rich tholeiitic magma will be minimal.
2. The Fe isotopic composition of a multiply saturated magma is unlikely to change significantly during fractional crystallization of magnetite if there is *competing* fractionation of other Fe-bearing cumulus phases (in particular, olivine and pyroxene). Therefore, it is fundamentally important to consider both the modal mineralogy and contribution of FeO by each phase to the whole rock when interpreting whole rock Fe isotopic data of cumulate rocks.

Acknowledgments
All data that support the conclusions of this paper can be found in the figures and tables included here. Any data not produced by the authors are cited by the original published work. A working, annotated example of the model is provided in the supporting information. The authors would like to thank Laura Sammon for her help in sample separation and Norbert Gajos for his help during some of the analyses. Helpful reviews from Helen Williams, Franck Poitrasson, Paolo Sossi, and 1 anonymous reviewer greatly improved the manuscript, as did the editorial handling of Janne Blichert-Toft.

References

Cawthorn, R. G., and L. D. Ashwal (2009), Origin of anorthosite and magnetitite layers in the Bushveld Complex, constrained by major element compositions of plagioclase, *J. Petrol.*, *50*, 1607–1637, doi:10.1093/petrology/egp042.

Cawthorn, R. G., and T. S. McCarthy, (1980), Variations in Cr content of magnetite from the upper zone of the Bushveld complex: Evidence for heterogeneity and convection currents in magma chambers, *Earth Planet. Sci. Lett.*, *46*, 335–343, doi:10.1016/0012-821X(80)90049-7.

Chen, L.-M., X.-Y. Song, X.-K. Zhu, X.-Q. Zhang, S.-Y. Yu, and J.-N. Yi, (2014), Iron isotope fractionation during crystallization and sub-solidus reequilibration: Constraints from the Baima mafic layered intrusion, SW China, *Chem. Geol.*, *380*, 97–109, doi:10.1016/j.chemgeo.2014.04.020.

Craddock, P. R., and N. Dauphas (2011), Iron isotopic compositions of geological reference materials and chondrites, *Geostand. Geoanal. Res.*, *35*, 101–123, doi:10.1016/j.epsl.2013.01.011.

Dauphas, N., P. R. Craddock, P. D. Asimow, V. C. Bennett, A. P. Nutman, and D. Ohnenstetter (2009), Iron isotopes may reveal the redox conditions of mantle melting from Archean to present, *Earth Planet. Sci. Lett.*, *299*, 255–267, doi:10.1016/j.epsl.2009.09.029.

Dauphas, N., et al. (2014), Magma redox and structural controls on iron isotope variations in Earth's mantle and crust, *Earth Planet. Sci. Lett.*, *308*, 127–140, doi:10.1016/j.epsl.2014.04.033.

Dziony, W., I. Horn, D. Lattard, J. Koepke, G. Steinhoefel, J. A. Schuessler, and F. Holtz (2014), In-situ Fe isotope ratio determination in Fe-Ti oxides and sulfides from drilled gabbros and basalt from the IODP Hole 1256D in the eastern equatorial Pacific, *Chem. Geol.*, *363*, 101–113, doi:10.1016/j.chemgeo.2013.10.035.

Fischer L. A., M. Wang, B. Charlier, O. Namur, R. J. Roberts, I. V. Veksler, R. G. Cawthorn, and F. Holtz (2016), Immiscible iron- and silica-rich liquids in the Upper Zone of the Bushveld Complex, *Earth Planet. Sci. Lett.*, *443*, 108–117.

Foden, J., P. A. Sossi, and C. M. Wawryk (2015), Fe isotopes and the contrasting petrogenesis of A-, I- and S-type granite, *Lithos*, *212-215*, 32–44, doi:10.1016/j.lithos.2014.10.015.

Harney, D. M. W., and G. von Gruenewaldt (1995), Ore-forming processes in the upper part of the Bushveld Complex, South Africa, *J. Afr. Earth Sci.*, *20*, 77–89.

Heimann A., B. L. Beard, and C. M. Johnson (2008), The role of volatile exsolution and sub-solidus fluid/rock interactions in producing high $^{56}Fe/^{54}Fe$ ratios in siliceous igneous rocks, *Geochim. Cosmochim. Acta*, *72*, 4379–4396, doi:10.1016/j.gca.2008.06.009.

Huang, F., P. Chakraborty, C. C. Lundstrom, C. Holmden, J. J. G. Glessner, S. W. Kieffer, and C. E. Lesher (2010), Isotope fractionation in silicate melts by thermal diffusion, *Nature*, *464*, 396–400, doi:10.1038/nature08840.

Irvine, T. N., and M. R. Sharpe (1986), Magma mixing and the origin of stratiform oxide ore zones in the Bushveld and Stillwater Complexes, in *Metallogeny of Basic and Ultrabasic Rocks*, edited by M. J. Gallagher, et al., pp. 183–198, Inst. of Min. Metall., London, U. K.

Klemm, D. D., R. Snethlage, R. M. Dehm, J. Henchel, and R. Schmidt-Thomé (1982), The formation of chromite and titanomagnetite deposits within the Bushveld Igneous Complex, in *Ore Genesis: The State of the Art, Special Publication of the Society for Geology Applied to Mineral Deposits*, vol. 2, edited by G. C. Amstutz, pp. 351–370, Springer, Berlin, doi:10.1007/978-3-642-68344-2_35.

Kruger, F. J., R. G. Cawthorn, and K. L. Walsh (1987), Strontium isotopic evidence against magma addition in the Upper Zone of the Bushveld Complex, *Earth Planet. Sci. Lett.*, *84*, 51–58, doi:10.1016/0012-821X(87)90175-0.

Liang, Y., C. Sun, L. D. Ashwal, and J. A. VanTongeren (2013), Spatial variations in temperature across the Bushveld layered intrusion revealed by REE-in-plagioclase-pyroxene thermometers with implications for magma chamber processes, Abstract V54B-07 presented at 2013 Fall Meeting, AGU, San Francisco, Calif.

Liu, P.-P., M.-F. Zhou, B. Luais, D. Cividini, and C. Rollion-Bard (2014), Disequilibrium iron isotopic fractionation during the high-temperature magmatic differentiation of the Baima Fe-Ti oxide-bearing mafic intrusion, SW China, *Earth Planet. Sci. Lett.*, *399*, 21–29, doi:10.1016/j.epsl.2014.05.0220012-821X.

Lundstrom, C. C. (2009), Hypothesis for the origin of convergent margin granitoids and Earth's continental crust by thermal migration zone refining, *Geochim. Cosmochim. Acta*, *73*, 5709–5729, doi:10.1016/j.gca.2009.06.020.

Mathez, E. A., J. A. VanTongeren, and J. Schweitzer (2013), On the relationships between the Bushveld Complex and its felsic roof rocks, part 1: Petrogenesis of Rooiberg and related felsites, *Contrib. Mineral. Petrol.*, *166*, 435–449, doi:10.1007/s00410-013-0884-3.

Millet, M., J. Baker, and C. Payne (2012), Ultra-precise stable Fe isotope measurements by high resolution multi-collector inductively coupled plasma mass spectrometry with a ^{57}Fe-^{58}Fe double spike, *Chem. Geol.*, *304-305*, 18–25, doi:10.1016/j.chemgeo.2012.01.021.

Molyneux, T. G. (1974), A geological investigation of the Bushveld Complex in Sekhukhuneland and part of the Steelpoort Valley, *Trans. Geol. Soc. S. Afr.*, *77*, 329–338.

Poitrasson, F. (2006), On the iron isotope homogeneity level of the continental crust, *Chem. Geol.*, *235*, 195–200, doi:10.1016/j.chemgeo.2006.06.010.

Poitrasson, F., and R. Freydier (2005), Heavy iron isotope composition of granites determined by high resolution MC-ICP-MS, *Chem. Geol.*, *222*, 132–147, doi:10.1016/j.chemgeo.2005.07.005.

Polyakov, V. B. and S. D. Mineev (2000), The use of Mössbauer spectroscopy in stable isotope geochemistry, *Geochim. Cosmochim. Acta*, *64*, 849–865.

Polyakov, V. B., R. N. Clayton, J. Horita, and S. D. Mineev (2007), Equilibrium iron isotope fractionation factors of minerals: Reevaluation from the data of nuclear inelastic resonant X-ray scattering and Mössbauer spectroscopy, *Geochim. Cosmochim. Acta*, *71*, 3833–3846, doi:10.1016/j.gca.2007.05.019.

Reynolds, I. M. (1985), The nature and origin of titaniferous magnetite-rich layers in the upper zone of the Bushveld Complex: A review and synthesis, *Econ. Geol.*, *80*, 1089–1108.

Roskosz M., C. K. I. Cio, N. Dauphas, W. Bi, F. L. H. Tissot, M. Y. Hu, J. Zhao, and E. E. Alp (2015), Spinel-olivine-pyroxene equilibrium iron isotopic fractionation and applications to natural peridotites, *Geochim. Cosmochim. Acta*, *169*, 184–199, doi:10.1016/j.gca.2015.07.035.

Schoenberg, R., M.A.W. Marks, J.A. Schuessler, F. von Blanckenburg, and G. Markl (2009), Fe isotope systematics of coexisting amphibole and pyroxene in the alkaline igneous rock suite of the Ilimaussaq Complex, South Greenland, *Chem. Geol.*, *258*, 65–77, 10.1016/j.chemgeo.2008.06.023.

Schuessler, J. A., R. Schoenberg, H. Behrens, and F. von Blanckenburg (2007), The experimental calibration of the iron isotope fractionation factor between pyrrhotite and peralkaline rhyoltic melt, *Geochim. Cosmochim. Acta*, *71*, 417–433, doi:10.1016/j.gca.2006.09.012.

Schuessler, J. A., R. Schoenberg, and O. Sigmarsson (2009), Iron and lithium isotope systematics of the Hekla volcano, Iceland: Evidence for Fe isotope fractionation during magma differentiation, *Chem. Geol.*, *258*, 78–91, doi:10.1016/j.chemgeo.2008.06.021.

Scoon, R. N., and A. A. Mitchell (1994), Discordant iron-rich ultramafic pegmatites in the Bushveld Complex and their relationship to iron-rich intercumulus and residual liquids, *J. Petrol.*, *35*, 881–917.

Shahar, A., E. D. Young, and C. E. Manning (2008), Equilibrium high-temperature Fe isotope fractionation between fayalite and magnetite: An experimental calibration, *Earth Planet. Sci. Lett.*, *268*, 330–338, doi:10.1016/j.epsl.2008.01.026.

Sossi, P. A. and H. O'Neill (2017), The effect of bonding environment on iron isotope fractionation between minerals at high temperature, *Geochim. Cosmochim. Acta*, *196*, 121–143, doi:10.1016/j.gca.2016.09.017.

Sossi, P. A., J. D. Foden, and G. P. Halverson (2012), Redox-controlled iron isotope fractionation during magmatic differentiation: An example from the Red Hill intrusion, S. Tasmania, *Contrib. Mineral. Petrol.*, *164*, 757–779, doi:10.1007/s00410-012-0769-x.

Sun, C., Y. Liang, L. Ashwal, and J. VanTongeren (2013), Temperature variations along stratigraphic height across the Bushveld Complex with implications for magma chamber processes in layered intrusions, *Geol. Soc. Am. Abstr. Programs*, *45*, 390.

Tegner, C., R. G. Cawthorn, and F. J. Kruger (2006), Cyclicity in the Main and Upper Zones of the Bushveld Complex, South Africa: Crystallization from a Zoned Magma Sheet, *J. Petrol.*, *47*, 2257–2279, doi:10.1093/petrology/egl043.

Telus, M., N. Dauphas, F. Moynier, F. L. H. Tissot, F-Z. Teng, P. I. Nabelek, P. R. Craddock, and L. A. Groat (2012), Iron, zinc, magnesium and uranium isotopic fractionation during continental crust differentiation: The tale from migmatites, granitoids, and pegmatites, *Geochim. Cosmochim. Acta*, *97*, 247–265, doi:10.1016/j.gca.2012.08.024.

Teng, F., N. Dauphas, and R. T. Helz (2008), Iron isotope fractionation during magmatic differentiation in Kilauea Iki Lava Lake, *Science*, *320*, 1620–1622, doi:10.1126/science.1157166.

Teng, F., W. F. McDonough, R. L. Rudnick, and R. J. Walker (2011), Diffusion-driven extreme lithium isotopic fractionation in country rocks of the Tin Mountain pegmatite, *Earth Planet. Sci. Lett.*, *243*, 701–710, doi:10.1016/j.epsl.2006.01.036.

VanTongeren, J. A., and E. A. Mathez (2012), Large-scale liquid immiscibility at the top of the Bushveld Complex, *Geology*, *40*, 491–494, doi:10.1130/G32980.1.

VanTongeren, J. A., and E. A. Mathez (2013), Incoming magma composition and style of recharge below the Pyroxenite Marker, Eastern Bushveld Complex, South Africa, *J. Petrol.*, *54*, 1585–1605, doi:10.1093/petrology/egt024.

VanTongeren, J. A., E. A. Mathez, and P. B. Kelemen (2010), A felsic end to Bushveld differentiation, *J. Petrol.*, *51*, 1891–1942, doi:10.1093/petrology/egq042.

Wang, K. (2013), Iron isotope cosmochemistry, PhD dissertation, Dept. Earth and Planet. Sci., Wash. Univ., in St. Louis, St. Louis, Washington, D. C.

Williams, H. M., A. H. Peslier, C. McCammon, A. N. Halliday, S. Levasseur, N. Teutsch, and J.-P. Burg (2005), Systematic iron isotope variations in mantle rocks and minerals: The effects of partial melting and oxygen fugacity, *Earth Planet. Sci. Lett.*, *235*, 435–452, doi:10.1016/j.epsl.2005.04.020.

Wombacher F., A. Eisenhauer, A. Heuser, and S. Weyer (2009), Separation of Mg, Ca and Fe from geological reference materials for stable isotope ratio analyses by MC-ICP-MS and double-spike TIMS, *J. Anal. At. Spectrom.*, *24*, 627–636, doi:10.1039/B820154D.

Young, E. D., C. E. Manning, E. A. Schauble, A. Shahar, C. A. Macris, C. Lazar, and M. Jordan (2015), High-temperature equilibrium isotope fractionation of non-traditional stable isotopes: Experiments, theory, and applications, *Chem. Geol.*, *395*, 176–195, doi:10.1016/j.chemgeo.2014.12.0130009-2541.

Zambardi, T., C. C. Lundstrom, X. Li, and M. McCurry (2014), Fe and Si isotope variations at Cedar Butte volcano; insight into magmatic differentiation, *Earth Planet. Sci. Lett.*, *405*, 169–179, doi:10.1016/j.epsl.2014.08.020.

Zhu D., B. Huiming, and Y. Liu (2015), Non-traditional stable isotope behaviors in immiscible silica-melts in a mafic magma chamber. *Nature, Scientific Reports*, doi:10.1038/srep175.